87 A PARAMETRIC WIND-PRESSURE RELATIONSHIP FOR RANKINE VS NON-RANKINE CYCLOSTROPHIC VORTICES

Vincent T. Wood[1] and Luther W. White[2]
[1]NOAA/OAR/National Severe Storms Laboratory, Norman, Oklahoma
[2]Department of Mathematics, University of Oklahoma, Norman, Oklahoma

1. INTRODUCTION

Attempts to interpret observed tangential wind and pressure distributions arising in dust devils, waterspouts, tornadoes, and mesocyclones from available observational data (e.g., mobile Doppler radar) have been made using an idealized, inviscid Rankine (Rankine 1882) vortex model. The simple Rankine vortex (henceforth RV) model coupled with the cyclostrophic balance assumption has been widely used by numerous investigators to provide an analytical model for the observed tangential wind and pressure structures in dust devils (Sinclair 1973; Cantor et al. 2006), waterspouts (Leverson et al. 1977), tornadoes (Hoecker 1961; Wakimoto and Wilson 1989; Winn et al. 1999; Lee and Wurman 2005), and misocyclones (Inoue et al. 2011). The model's inner and outer tangential wind profiles can be modified to fit fairly well the available observational data; however, the profile's unrealistic cusp at the core radius remains unchanged and is usually ignored. The result is that the discontinuous tangential velocity peak is overestimated and is not well matched with the observed continuous tangential wind maximum. This problem gives rise to a vital question as to how varying the radial profiles of the RV tangential wind affects the pressure deficits within the vortex core region when the cusp is unable to match the broadly peaked wind profile. The RV model with cyclostrophic flow, for instance, explained about 75% of the in-situ pressure deficit measurements in the vicinity of dust devils (Sinclair 1973) and waterspouts (Leverson et al. 1977). This discrepancy could be attributed to the neglect of radial and vertical components of flow in the model. For a given tangential velocity maximum, Fiedler (1994), however, showed that his non-Rankine vortex[1] (henceforth non-RV) has a central pressure deficit twice that of the RV, suggesting that varying tangential wind profiles in the non-RV model have an important modulating influence on the behavior of pressure profiles. The profiles underscore the limitation of the RV model for many applications because of the mathematical simplicity in the model. The profiles underscore the limitation of the RV model for many applications because of the mathematical simplicity in the model. Consequently, the inadequacy of the model provides motivation to apply the Wood and White (2011) parametric tangential-wind profile model to a wind-pressure relationship and to determine whether the model can better fit realistic pressure deficit profiles than the RV model does.

The objective of this paper is to develop a parametric model of wind-pressure profiles by applying the Wood-White (WW) model to the cyclostrophic wind-pressure relationship of an assumed axisymmetric vortex. Analytical tangential wind profiles in the RV and non-RV models are described in section 2. In section 3, a mathematical description of pressure deficits obtained, via this relationship, in the RV and non-RV (WW) models is presented. Section 4 elucidates the roles of the shape velocity parameters in the behaviors of the radial distributions of tangential winds and pressure deficits of the RV vs. non-RV models for comparison. A summary of the analytical results is discussed in section 5.

2. ANALYTICAL TANGENTIAL WIND PROFILES

2.1 Rankine Vortex Tangential-Wind Profile

A classic model of inviscid vortex flow is the idealized, steady-state Rankine vortex that frequently is used as a first approximation to an atmospheric vortex. It consists of tangential velocity that increases linearly from zero at the center of the vortex to a maximum value at the core radius (solidly rotating core region) and then decreases, with velocity being inversely proportional to distance from the center. Tangential velocity, V_{RV}, is expressed as a function of radius, r, as

$$V_{RV}^{*} \equiv \frac{V_{RV}}{V_X} = \rho^{\mu}, \qquad (1)$$

where V_X is the peak tangential velocity that occurs at the core radius R_X, $\rho \equiv r / R_X$ is the dimensionless radius, and μ is an exponent that is equal to 1 within the core region ($\rho \le 1$) and equal to –1 outside the core region ($\rho > 1$). The exponent can be modified to describe different shapes of the inner and outer profiles. In their proximity radar observations of tornadoes by mobile, high-resolution Doppler radars, Wurman and Gill (2000), Wurman (2002), and Wurman and Alexander (2005), for instance, used the tangential wind profiles of the Rankine model to closely match the inner cores of solid-body rotation – in some cases, to the inner radial profiles of Doppler velocities. Outside the cores, they observed Doppler velocity profiles of $V \propto r^{-0.6\pm0.1}$. The

[1] The "non-Rankine vortex" may be defined as a viscous vortex which exhibits a smooth transition between solid-body rotation and potential flow that encompasses the annular zone of the velocity maximum, resembling the viscous Burgers-Rott tangential velocity profile.

Corresponding author address: Vincent T. Wood, National Severe Storms Laboratory, 120 David L. Boren Blvd., Norman, Oklahoma 73072, USA; e-mail: Vincent.Wood@noaa.gov

Rankine vortices with varying exponents will be used to compare against non-Rankine vortices that are described in the subsequent subsections.

2.2 Wood-White Parametric Tangential-Wind Profile

The simple non-Rankine vortex may be modeled using the parametric tangential-wind (V_{WW}) profile of Wood and White (2011). The profile for inviscid, axisymmetric flow is expressed by

$$V_{WW}^{*} \equiv \frac{V_{WW}(\rho;\mathrm{m})}{V_X} = \frac{\eta^{\lambda}\rho^{\kappa}}{(\eta-\kappa+\kappa\rho^{\eta/\lambda})^{\lambda}},\ 1\le\kappa<\eta,\ \lambda>0. \quad (2)$$

The WW profile employs a model vector of five key parameters: $\mathrm{m}=[V_X, R_X, \kappa, \eta, \lambda]^{\mathrm{T}}$, where V_X and R_X have been defined previously, and κ, η and λ represent different shape velocity parameters that are related to different shapes of the velocity profile. Note that κ and η are the same parameters "k" and "n" as initially developed by Wood and White (2011).

The radial profile families of normalized tangential velocity (V_{WW}^{*}) as functions of κ, η and λ are schematically presented in Fig. 1. The κ parameter may be thought of the *growth* parameter since it controls a linearity or nonlinearity of the inner velocity profile near the vortex center ($\rho=0$). When $\kappa=1$, the linear profile is V-shaped and is related to the inner core of solid-body rotation (Figs. 1a, 1d, 1g). As κ becomes large (i.e., as one progresses from left to right panels of the figure), the curvature of the profile progressively changes such that the V-shaped profile (left column of Fig. 1) transitions into the bowl-shaped profile (center column) and eventually into the U-shaped profile (right column). At the same time, the width of zero tangential velocity increases at the vortex center.

The η parameter may be thought of the *decay* parameter since it controls the size of the decaying outer velocity profile (Fig. 1). In each panel of the figure, three varying values of η are presented for each fixed value of κ and λ. The higher the η value, the more rapidly the outer profile decreases with ρ beyond $\rho=1$.

The λ parameter may be thought of the *size* parameter since it controls the radial width of the velocity profile in the annular zone of the maximum. When $\lambda=1$, a broadly peaked profile results (Fig. 1). As $\lambda\to0$, three radial profiles for different η values merge together in each panel to form one superimposed radial profile at $\rho\le1$. Simultaneously, the profile transitions to a sharply peaked profile that resembles the modified Rankine velocity profile. Both κ and η alone cannot allow adjustment of the sharp profile at $\rho=1$. To show how (2) coincides with the modified RV tangential velocity in (1) as shown in the bottom panels of Fig. 1, we follow the approach of Wood and White (2011) by taking the limit of (2) as $\lambda\to0$. Thus,

$$\lim_{\lambda\to0} V_{WW}^{*} = \begin{Bmatrix} \rho^{\kappa} \\ \rho^{(\kappa-\eta)} \end{Bmatrix} = V_{RV}^{*},\ \begin{matrix}\rho\le1,\\ \rho\ge1,\end{matrix}\ 1\le\kappa<\eta. \quad (3)$$

The κ and η are easily determined by setting ρ^{μ} in (1) equal to (3) and then taking the natural logarithm of the result which yields

$$\begin{matrix}\kappa\\ \kappa-\eta\end{matrix}\Bigg\} = \mu = \begin{cases}1, & \rho\le1\\ -1, & \rho\ge1\end{cases}. \quad (4)$$

When $\kappa=\mu=1$, for example, V_{WW}^{*} increases linearly from a circulation center to $\rho=1$. When $\mu=-1$, $\eta=\kappa-\mu=\kappa+1$, meaning that V_{WW}^{*} is inversely proportional to ρ beyond $\rho=1$ (potential flow). The RV model in (1) may be viewed as a limiting case for the non-RV (WW) model as $\lambda\to0$.

3. WIND-PRESSURE RELATIONSHIP FOR A CYCLOSTROPHIC VORTEX

Since the horizontal scale of an atmospheric vortex is small (e.g., a tornado), the Coriolis force can be neglected in the horizontal momentum equation (i.e., high Rossby numbers). In an axisymmetric vortex, assumption of balance between central pressure and wind speed, termed cyclostrophic balance, is given by

$$\alpha_o \frac{\partial P(r)}{\partial r} = \frac{V_C^2(r)}{r}, \quad (5)$$

where $V_C(r)$ is the cyclostrophic (tangential) velocity, $P(r)$ is the radial pressure fluctuation from that of the motionless, equilibrium state multiplied by the constant specific volume of air α_o. The pressure deficit ΔP is obtained by integrating (5) radially inward from an environmental pressure $P_e[=P(r\to\infty)]$ at which the tangential winds decrease asymptotically to zero infinitely far from the vortex center, and is given by

$$\Delta P(r) = P(r) - P_e = \alpha_o^{-1}\int_{\infty}^{r} \frac{V_C^2(s)}{s}\,ds. \quad (6)$$

Note that s is a dummy variable for the integration. Integration of (6) is done numerically in all but simple cases. (6) involves the inward integral which is calculated using the trapezoidal rule (e.g., Press et al. 1992, p. 125-126). Using (6), the cyclostrophic wind balance for the vortex is employed to derive a pressure profile from a varying non-RV tangential wind profile as functions of κ, η and λ, as will be presented in the subsequent sections.

To facilitate comparison with the profiles, normalized composites were constructed that preserved the underlying tangential wind and pressure structures. Each individual profile was expressed in the convenient dimensionless form utilizing the typical scales V_X and

R_X. A profile of ΔP_{WW}^* for the non-Rankine vortex is obtained by incorporating $V_C = V_{WW}$ in (2) into (6), dividing the result by $\alpha_o^{-1} V_X^2$, and integrating the further result. Thus, it is expressed by

$$\Delta P_{WW}^*(\rho) \equiv \frac{\Delta P_{WW}(\rho)}{\alpha_o^{-1} V_X^2} = \int_{\infty}^{\rho} \frac{\eta^{2\lambda} s^{(2\kappa-1)}}{[\eta - \kappa + \kappa s^{(\eta/\lambda)}]^{2\lambda}} ds . \qquad (7)$$

A normalized pressure deficit (ΔP_{RV}^*) for the RV is derived by incorporating $V_C^* = V_{RV}^*$ in (1) into (7) and integrating the result inward radially in a piecewise manner (that is, from ∞ to $\rho = 1$ and also from $\rho = 1$ to $\rho < 1$). Thus, ΔP_{RV}^* is obtained as

$$\lim_{\lambda \to 0} \Delta P_{WW}^*(\rho) = \Delta P_{RV}^*(\rho) \equiv \frac{\Delta P_{RV}(\rho)}{\alpha_o^{-1} V_X^2} = \qquad (8)$$

$$\begin{cases} \int_1^{\rho} s^{2\kappa-1} ds + \int_{\infty}^{1} s^{2(\kappa-\eta)-1} ds = \dfrac{\rho^{2\kappa} - 1}{2\kappa} + \dfrac{1}{2(\kappa-\eta)}, & \rho \le 1, \\ \int_{\infty}^{\rho} s^{2(\kappa-\eta)-1} ds = \dfrac{\rho^{2(\kappa-\eta)}}{2(\kappa-\eta)}, & \rho \ge 1. \end{cases}$$

Note on the top-hand side of (8) that $\Delta P_{RV}^*(\rho)$ must change continuously at $\rho = 1$ between the inner ($\rho \le 1$) and outer ($\rho \ge 1$) tangential velocity profiles. A few values of the model parameters (κ, η, λ) are selected to investigate the effects of the cyclostrophic winds on the behavior of pressure deficits in order to compare against the radial profiles of the Rankine tangential wind and pressure deficit, as will be shown in the later section.

4. RADIAL PROFILES OF TANGENTIAL VELOCITY AND PRESSURE DEFICIT IN THE RANKINE AND NON-RANKINE VORTICES

Figures 2-5 provide what the model parameters (κ, η, λ) may deduce about the non-RV tangential wind and pressure deficit changes when comparing against the radial distributions of the RV tangential velocity and pressure deficit. We performed comparative experiments by varying the size parameter (λ) while keeping the growth (κ) and decay (η) parameters unchanged in the radial distributions of the non-RV tangential velocity and pressure deficit (Fig. 2). Note that the selected values of κ, η and λ are shown in the lower panel of the figure. The values were used as inputs to calculate (1)-(2), (7) and (8) to produce such profiles. When κ and η remain constant, different inner and outer velocity profiles controlled by various λ values have an important influence on the behavior of pressure deficit profiles. As $\lambda \to 0$, the non-RV tangential velocity and pressure deficit profile coincide with those of the RV. For a given tangential velocity maximum, vortex A (red curve) has twice the central pressure deficit of the RV, owing to the broadly peaked profile of vortex A.

We now investigate the role of the growth parameter (κ) in the behavior of the radial profiles of tangential velocity and pressure deficit (Fig. 3). By keeping η and λ fixed, different inner velocity profiles controlled by different κ values can have an impact on the behavior of the pressure deficit profiles, as comparison between Figs. 2 and 3 shows. At a given value of λ, a transition from a V-shaped to a U-shaped profile of tangential velocity inside $\rho = 1$ produces a change in the corresponding pressure deficit profiles (Fig. 3). At the vortex center, the pressure profile is flat, while at the same time, the central pressure deficit fills. Outside $\rho = 1$, the outer profiles appear to be relatively insensitive to variations in κ because this parameter is dominant near the vortex center.

As $\lambda \to 0$ and κ and η remain unchanged, the non-RV tangential velocity and pressure deficit distributions agree with those of the RV. For a given tangential velocity maximum, vortex D (red curve in Fig. 3) has the central pressure deficit about half that of the RV (gray curve), owing to the drastic reduced tangential velocity profile inside the radius of the maximum.

Now that we comprehend how the different κ variables at a given value of λ control the inner profiles, we further explore the role of the decay parameter (η) in influencing the radial distributions of tangential velocity and pressure deficit (Fig. 4). Comparing to the $\eta = 2.0$ (Fig. 2), this η is reduced to 1.5, indicating the slow decay of the outer tangential velocity profile (Fig. 4). Various outer velocity profiles controlled by different η values can have an impact on the behavior of the pressure deficit profiles, as dual inspection of Figs. 2 and 4 evidently illustrates. When κ is fixed, decreasing η causes the pressure profile to fall at a given value of λ. As $\lambda \to 0$, the non-RV tangential velocity and pressure deficit profiles concur with those of the RV. For a given tangential velocity maximum, vortex G (red curve in Fig. 4) has almost twice the central pressure deficit of the RV, owing to the slow decay of the outer tangential velocity profile. Inside $\rho = 1$, the inner profiles appear to be relatively insensitive to variations in η since this parameter is dominant beyond $\rho = 1$.

Suppose that an outer tangential wind profile decays very quickly. What would happen to the corresponding pressure deficit? This question can be answered by increasing the decay parameter (η) to 2.5 (Fig. 5). Comparing to the outer profiles of tangential velocity and pressure deficit (Figs. 2 and 4), the pressure deficit profiles (Fig. 5) are almost zero beyond approximately $\rho = 2.5$ at a given value of λ. Simultaneously, the

profiles drop slowly as one approaches $\rho = 0$ from far radius. This is owing to the quick decay of the outer profiles of tangential velocity. Vortex J (red curve) has twice the central pressure of the RV, as is similar to that of vortex A (Fig. 2) and vortex G (Fig. 4).

5. CONCLUSIONS

A parametric model of wind-pressure profiles is developed by applying the WW model to the wind-pressure relationship of a cylostrophic vortex. The experiments demonstrate that the model is capable of explaining significant fluctuations in tangential wind speeds and pressure deficits and may replicate the general aspects of observed profiles in dust devils, tornadoes, tornado cyclones and mesocyclones. The main conclusions of this study are as follows:

1) The shape velocity parameters (κ, η, λ) play a vital role in modulating all portions of the cyclostrophic wind profile. In our formulation, the profile is defined by (a) the growth parameter (κ) that predominantly dictates the inner wind profile near the vortex center, (b) the decay parameter (η) that primarily governs the outer profile beyond the radius of the tangential wind maximum, and (c) the size parameter (λ) that mainly determines the radial size of the velocity profile in the annular zone of the maximum.

2) The pressure deficits are sensitive to the shape velocity parameters in the cyclostrophic wind profile because the shape profile determines the wind-pressure relation. For a given tangential velocity maximum, a decrease (increase) in λ narrows (broadens) the tangential wind profile straddling the maximum. Also it raises (lowers) the corresponding pressure deficit profile and, hence, the central pressure minimum. Increasing (decreasing) the κ parameter changes the inner wind profile in such a way to not only raise (lower) the pressure profile but also increase (decrease) the width of the profile inside the radius of the tangential velocity peak. On the other hand, increasing (decreasing) the η parameter decreases (increases) the wind profile beyond the radius of maximum tangential velocity and increases (decreases) the pressure deficit profile. Furthermore, the central pressure deficits for given values of V_X , κ , η and λ at $\rho = 0$ remain unchanged, regardless of the vortex size.

3) When comparing to the non-Rankine central pressure deficit for a given tangential velocity maximum, the Rankine central pressure deficit profile is mismatched because the Rankine tangential wind profile's unrealistic cusp at the radius of the maximum remains unchanged and is not able to match the wind maximum, as commonly seen in various observations. It is suggested that the Rankine vortex model may not provide an analytical model for the observed tangential wind and pressure structures in dust devils, waterspouts, tornadoes and mesocyclones.

Acknowledgments. We appreciate the constructive comments on this manuscript provided by Qin Xu and Robin Tanamachi of NSSL.

6. REFERENCES

Fiedler, B. H., 1994: The thermodynamic speed limit and its violation in axisymmetric numerical simulations of tornado-like vortices. *Atmos.-Ocean,* **32,** 335-359.

Hoecker, Jr., W. H., 1961: Three-dimensional pressure pattern of the Dallas tornado and some resultant implications. *Mon. Wea. Rev.,* **89,** 533-542.

Inoue, H. Y., K. Kusunoki, W. Kato, H. Suzuki, T. Imai, T. Takemi, K. Bessho, M. Nakazato, S. Hoshino, W. Mashiko, S. Hayashi, T. Fukuhara, T. Shibata, H. Yamauchi, and O. Suzuki, 2011: Finescale Doppler radar observations of a tornado and low-level misocyclones within a winter storm in the Japan Sea coastal region. *Mon. Wea. Rev.,* **139,** 351-369.

Lee, W.-C., and J. Wurman, 2005: Diagnosed three-dimensional axisymmetric structure of the Mulhall tornado on 3 May 1999. *J. Atmos. Sci.,* **62,** 2373-2393.

Leverson, V. H., P. C. Sinclair, and J. H. Golden, 1977: Waterspout wind, temperature, and pressure structure deduced from aircraft measurements. *Mon. Wea. Rev.,* **105,** 715-733.

Rankine, W. J. M., 1882: *A Manual of Applied Physics.* 10th ed., Charles Griff and Co., 663 pp.

Sinclair, P. C., 1973: The lower structure of dust devils. *J. Atmos. Sci.,* **30,** 1599-1619.

Wakimoto, R. M., and J. W. Wilson, 1989: Non-supercell tornadoes. *Mon. Wea. Rev.,* **117,** 1113-1140.

Wood, V. T., and L. W. White, 2011: A new parametric model of vortex tangential-wind profiles: Development, testing, and verification. *J. Atmos. Sci.,* **68,** 990-1006.

Wood, V. T., L. W. White, H. E. Willoughby, and D. P. Jorgensen, 2012: A new parametric tropical cyclone tangential wind profile model. *Mon. Wea. Rev.* (In press.)

Wurman, J., 2002: The multiple-vortex structure of a tornado. *Wea. Forecasting,* **17,** 473-505.

Wurman, J., and S. Gill, 2000: Finescale radar observations of the Dimmitt, Texas (2 June 1995), tornado. *Mon. Wea. Rev.,* **128,** 2135-2164.

Wurman, J., and C. R. Alexander, 2005: The 30 May 1998 Spencer, South Dakota, storm. Part II: Comparison of observed damage and radar-derived winds in the tornadoes. *Mon. Wea. Rev.,* **133,** 97-119.

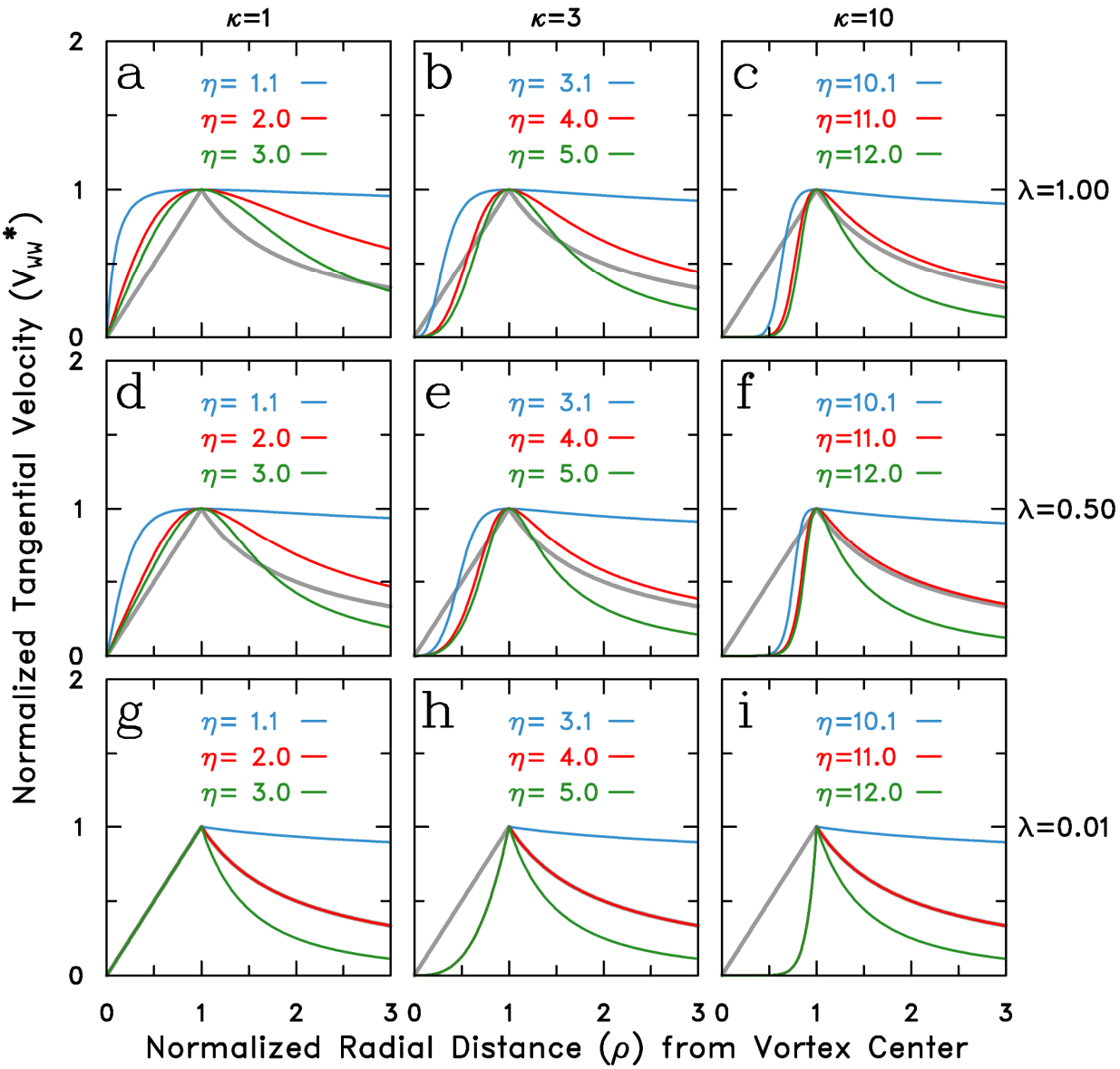

FIG. 1. Radial profile families of V_{WW}^* for selected values of κ, η and λ. Three profile families in each panel are indicated by three different values of η. The gray curve represents the Rankine velocity profile for comparison. Normalized radial distance is represented by $\rho \equiv r / R_X$. [From Wood and White (2011).]

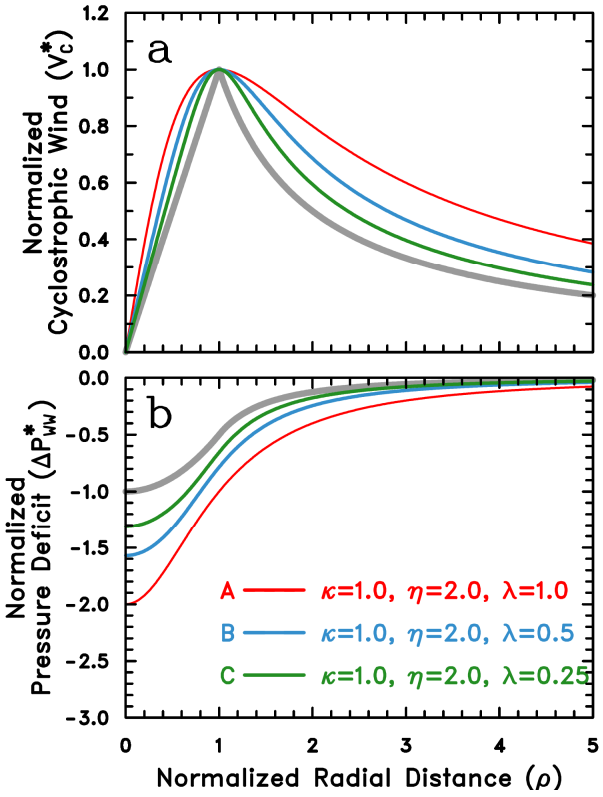

FIG. 2. Radial profiles of (a) tangential velocity and (b) corresponding pressure deficit as functions of κ, η and λ for non-Rankine vortices A (red curve), B (blue curve) and C (green curve). The profiles are normalized. Radial profile of Rankine vortex (gray curve) is indicated for comparison.

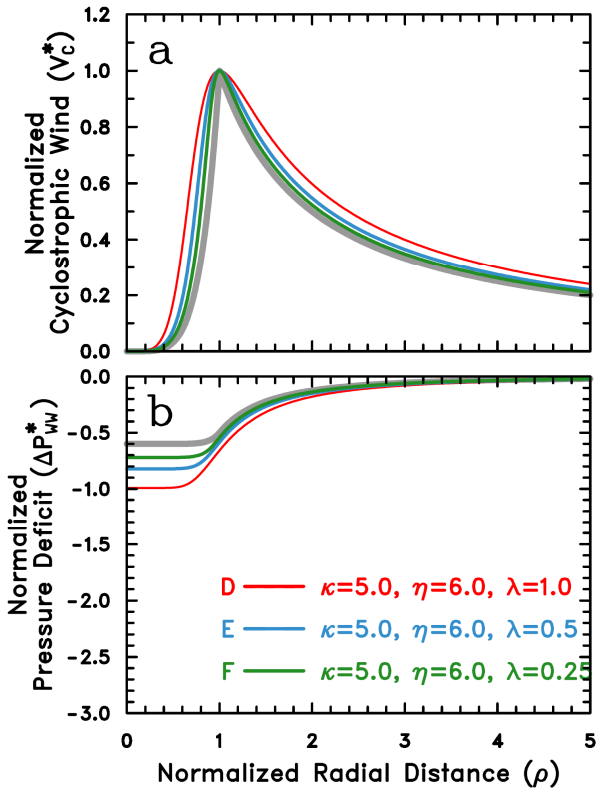

FIG. 3. Radial profiles of (a) tangential velocity and (b) corresponding pressure deficit as functions of κ, η and λ for non-Rankine vortices D (red curve), E (blue curve) and F (green curve). The profiles are normalized. Radial profile of Rankine vortex (gray curve) is indicated for comparison.

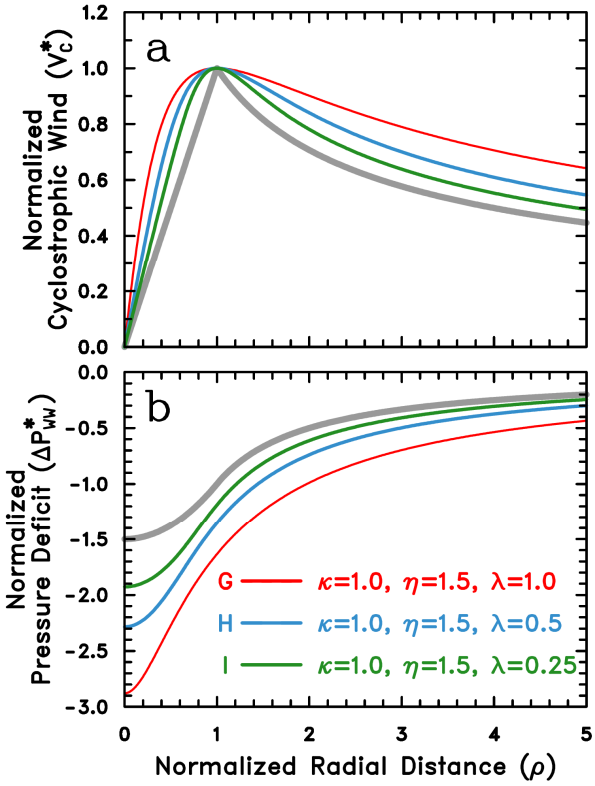

FIG. 4. Radial profiles of (a) tangential velocity and (b) corresponding pressure deficit as functions of κ, η and λ for non-Rankine vortices G (red curve), H (blue curve) and I (green curve). The profiles are normalized. Radial profile of Rankine vortex (gray curve) is indicated for comparison.

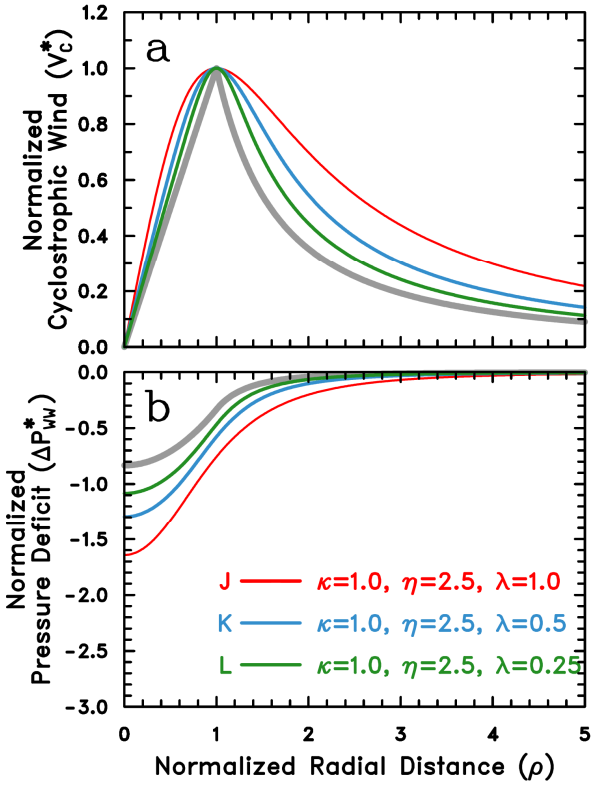

FIG. 5. Radial profiles of (a) tangential velocity and (b) corresponding pressure deficit as functions of κ, η and λ for non-Rankine vortices J (red curve), K (blue curve) and L (green curve). The profiles are normalized. Radial profile of Rankine vortex (gray curve) is indicated for comparison.